Hydraulic Control of Sill Flow with Bottom Friction*

L. J. PRATT**

Woods Hole Oceanographic Institution, Woods Hole, MA 02543

(Manuscript received 21 March 1986, in final form 11 June 1986)

ABSTRACT

The hydraulics of strait and sill flow with friction is examined using a reduced gravity model. It is shown that friction moves the critical (or control) point from the sill to a location downstream. If the strait has constant width, the control point lies where the bottom slope is the negative of the drag coefficient C_d. If $-C_d$ exceeds the bottom slope everywhere, the flow cannot be controlled (in the classical sense that energy and flow force are minimized). Friction also decreases the minimum obstacle height required to establish hydraulically controlled flow in the classical laboratory towing experiment. Also, friction greatly encourages the establishment of stationary hydraulic jumps in the lee of the sill and, under certain conditions, gives rise to stationary jumps on the upstream face of the obstacle. Some consequences of these results for deep-ocean overflows are given using the Iceland–Faroe overflow as an example.

1. Introduction

Open-channel hydraulic theory has been used extensively by oceanographers interested in the dynamics of strait and sill flow. Studies range in time from Stommel and Farmer's (1952) pioneering investigation of a two-layer exchange flow and Long's (1954) laboratory experiments with unidirectional sill flows to recent studies of dispersive and multilayered flows (e.g., Armi and Farmer, 1984; Baines, 1984; Pratt, 1984a; Lawrence, 1985; Farmer and Denton, 1985). With very few exceptions, the fluid flows investigated in these studies have been frictionless, a restriction that can be justified in some sea straits but is unrealistic in many others. The importance of bottom friction in a given strait can be roughly ascertained through the following argument. Suppose that a deep layer of water enters the strait from an upstream basin and is hydraulically controlled by a sill located in the strait. In longitudinal section the flow might look like the Iceland–Faroe overflow, which appears in Fig. 1. Let H and U be the mean thickness and velocity of the deep layer and L be the alongstream distance over which H and U change significantly due to hydraulic effects. Then U^2/L measures the parcel acceleration (which is crucial to the hydraulic control of the layer) through the strait, while C_dU^2/H measures the parcel deceleration due to friction, parameterized here using the dimensionless drag coefficient C_d. The relative importance of friction is thus indicated by C_dL/H, and approximate values of this parameter for several well-known sea straits, computed using a conservative[1] value $C_d = 10^{-3}$, are listed in Table 1. Most of the straits listed have $0.7 < C_dL/H < 2.0$, indicating that friction is important. The only strait listed in which friction is apparently weak is Gibraltar, with $C_dL/H = 0.1$.

The purpose here is to determine how friction changes the basic properties of hydraulically controlled flow and how control is exercised. Because hydraulic control is an essentially nonlinear process, it is extremely difficult to treat friction in a purely deductive way. Therefore, friction is parameterized using a quadratic law, and the analysis is carried only to the point of determining gross effects, rather than details. Attention is restricted to the hydraulics of single-layer flows with no rotation, the purpose being to lay the groundwork for the treatment of more difficult, multilayer and/or rotating flows. In particular, I will investigate the effect of friction on the mechanisms by which hydraulic control is exercised, the location of the point of control, the minimum sill height needed for control, and the existence of hydraulic jumps.

2. Review of inviscid hydraulics

Consider a layer of fluid of uniform density $\rho + \Delta\rho$ flowing steadily over an isolated obstacle of height b_m in a strait of rectangular cross section (see Fig. 2). Above this layer lies a deep inactive layer of density ρ. If the ratio of the obstacle height b_m to its length $2L$ is sufficiently small, the lower layer behaves according to the shallow water equations:

* Woods Hole Oceanographic Institution Contribution No. 6198.

** Current address: Scripps Institution of Oceanography, La Jolla, CA 92093.

[1] Recent direct measurements of C_d along the California shelf by Grant et al. (1984) show that C_d can be as large as 4.4×10^{-3}, indicating that the values in Table 1 may well be underestimates.

© 1986 American Meteorological Society

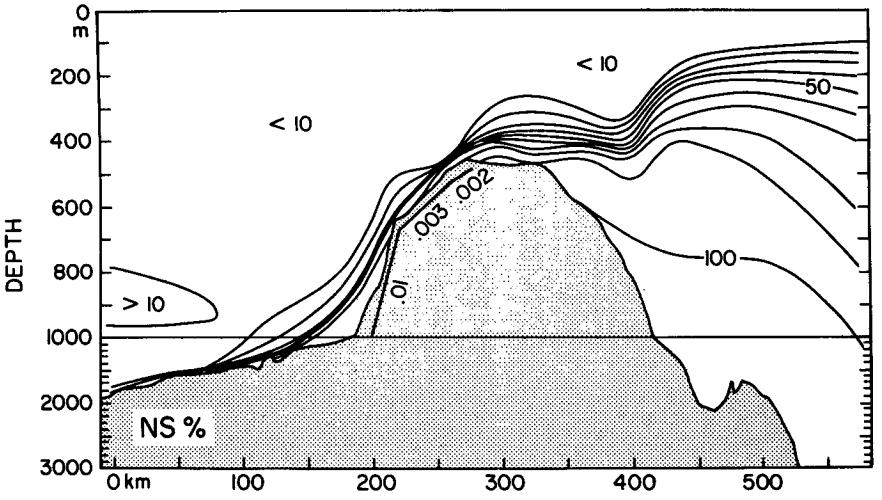

FIG. 1. Percent of Norwegian Sea deep water on section normal to the central Iceland–Faroe Ridge (from Hansen and Meincke, 1979). The flow is from right to left.

$$udu/dx + g^*dh/dx = -g^*db/dx - C_d u^2/h \quad (2.1)$$

$$hdu/dx + udh/dx = -w^{-1}uhdw/dx. \quad (2.2)$$

Here, h is the thickness or "depth" and u the depth-independent velocity of the active layer, g^* is gravity reduced in proportion to $\Delta\rho/\rho$, b is the bottom elevation, and w is the channel width. The effect of variations in bottom topography on the active layer are essentially the same as those of width variation, and w will therefore be made constant in all that follows. However, I will occasionally note the generalization of results to nonconstant w.

Integrating (2.1) and (2.2) from the point $x = -L$ at the upstream edge of the obstacle to a point x over the obstacle yields

TABLE 1. Values of C_dL/H for various sea straits: L the alongstream length, H the average layer depth, and $C_d = 10^{-3}$.

Sea strait	H (m)	L (m)	C_dL/H
Strait of Gibraltar Outflow (Lacombe and Richez, 1982)	2×10^2	2×10^4	0.1
Vema Channel (Hogg, 1983)	3×10^2	2×10^5	0.7
Bornholm Strait (Walin and Petren, 1976)	30	2.5×10^5	0.8
Denmark Strait (Grant, 1968)	5×10^2	5×10^5	1.0
Ecuador Trench (Lonsdale, 1977)	3×10^2	3×10^5	1.0
Iceland–Faroe Ridge (Hansen and Meincke, 1979)	4×10^2	4×10^5	1.0
Bering Strait (Stigebrandt, 1984)	50	10^5	2.0
Bosphorus (Tolmazin, 1977)	20	2×10^4	1.0

$$u^2(x)/2 + g^*[h(x) + b(x)] = u_1^2/2 + g^*h_1 - C_d\int_{-L}^{x}[u^2(\hat{x})/h(\hat{x})]d\hat{x} \quad (2.3)$$

$$u(x)h(x) = Q/w \quad (2.4)$$

where Q is the volume flow rate and $u_1 = u(-L)$, $h_1 = h(-L)$. Dividing (2.3) by g^*b_m to nondimensionalize and eliminating $u(x)$ using (2.4) yields an integral equation for the layer thickness:

$$\frac{q^2}{2}\left(\frac{b_m}{h}\right)^2 + \left(\frac{h}{b_m}\right) + \left(\frac{b}{b_m}\right) = B_1 - \alpha q^2\int_{-1}^{x/L}(b_m/h)^3 d(\hat{x}/L) \quad (2.5)$$

where

$$q = Q/(g^{*1/2}b_m^{3/2}w) \quad (= \text{dimensionless flow rate})$$

$$B_1 = (u_1^2/2 + g^*h_1)/g^*b_m \quad (= \text{dimensionless energy or Bernoulli function at } x = -L)$$

$$\alpha = C_dL/b_m \quad (= \text{friction parameter}).$$

The frictionless ($\alpha = 0$) solutions to (2.5) are well known and their salient features will now be summarized briefly. Suppose that one first specifies the topography and a value for the dimensionless flow rate q, then considers the different solutions obtained by varying the dimensionless upstream energy B_1. This has been done in Fig. 3 using $q = 1$ and a parabolic obstacle:

$$b = b_m[1 - (x/L)^2], \quad |x/L| < 1. \quad (2.6)$$

The figure shows the interface profiles for three values of B_1, and the profiles are distinguished primarily by their ability to support upstream wave propagation.

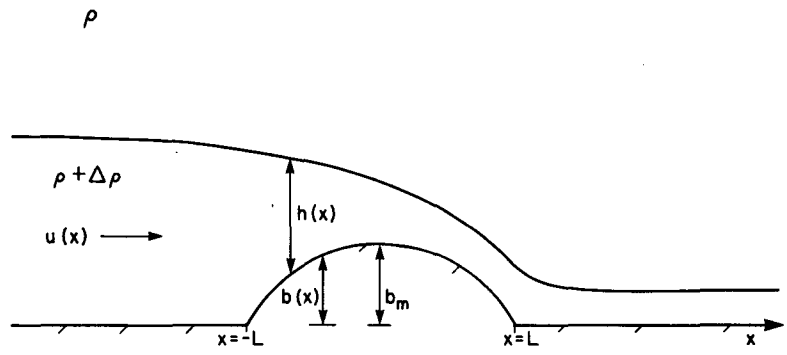

FIG. 2. Definition sketch.

An infinitesimal, long interfacial wave propagating against the current has speed

$$c_- = u - (g^*h)^{1/2} = \frac{b_m^{3/2} g^{*1/2}}{h}[q - (h/b_m)^{3/2}].$$

With $q = 1$ this speed clearly vanishes (the flow is critical) when $(h/b_m) = 1$. The solution labeled A–A′ in Fig. 3 is called subcritical since h/b_m is everywhere greater than unity, implying $c_- < 0$, and arrows have been drawn indicating that upstream propagation is allowed. Both this solution and the solution labeled D–D′ have the same upstream energy $B_1 = 2.86$. The latter is supercritical ($c_- > 0$) everywhere since h/b_m is everywhere less than unity. If B_1 is decreased, the solution curves go through a succession of subcritical and supercritical curves resembling A–A′ and D–D′ until the value $B_1 = 2.5$, and here the two curves intersect at $x = 0$. At the point of intersection the figure indicates that $h/b_m = 1$, so the flow is critical $c_- = 0$. For curve B–B′ of the intersecting solution, the flow is subcritical upstream of the sill and supercritical downstream. This solution is said to be hydraulically controlled, the term "control" having implications for the way in which this flow adjusts to time-dependent changes in bottom topography or upstream conditions, as discussed below. The second branch (curve C–C′) of the intersecting solution is unstable (see Pratt, 1984a) and has never been realized in the laboratory. Further decreases in the value of B_1 lead to solutions that are not continuous over the obstacle, as exemplified by curves E–E′ and F–F′ in Fig. 3. These solutions simply have insufficient energy to surmount the sill.

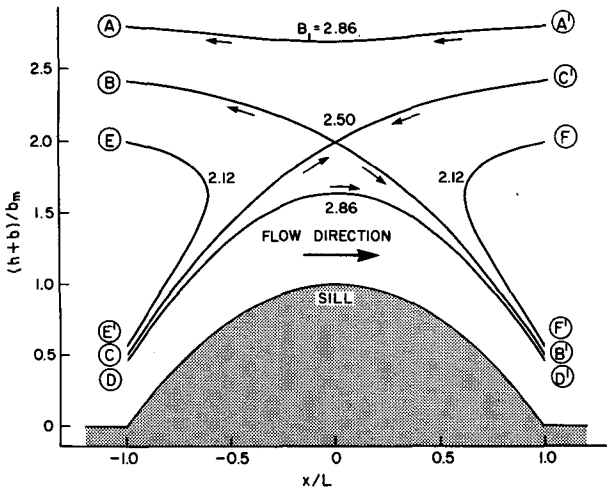

FIG. 3. Steady solutions over a parabolic obstacle with $\alpha = 0$. All solutions have the same dimensionless flow rate $q = 1$, but different energy constants B_1.

The hydraulically controlled solution (curve B–B′) has several features worth reviewing. From the proceeding discussion, it is already clear that this solution possesses the minimum energy necessary to surmount the obstacle. Also consider the dimensionless "flow force"

$$M(x/L) = [u^2h + g^*h^2/2]/(g^*b_m^2)$$
$$= q^2(b_m/h) + \tfrac{1}{2}(h/b_m)^2 \qquad (2.7)$$

and "specific energy":

$$E(x/L) = (u^2/2 + g^*h)/(g^*b_m)$$
$$= q^2(b_m/h)^2/2 + h/b_m \qquad (2.8)$$

both of which are plotted as functions of (h/b_m) for $q = 1$ in Fig. 4. Note from the figure that both E and M are minimal when the flow is critical (i.e., when $h/b_m = 1$):

$$\left.\frac{\partial M}{\partial(h/b_m)}\right|_{q=1} = 0, \quad \text{when } h/b_m = 1 \qquad (2.9)$$

$$\left.\frac{\partial E}{\partial(h/b_m)}\right|_{q=1} = 0, \quad \text{when } h/b_m = 1. \qquad (2.10)$$

In summary, the hydraulically controlled flow at the sill possesses the lowest flow force and specific energy of any point of any possible $q = 1$ solution, and the

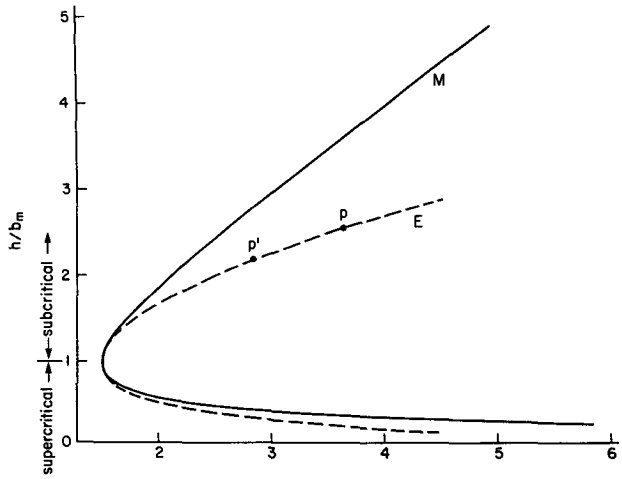

FIG. 4. Dimensionless specific energy E and flow force F as functions of depth h/b_m for $q = 1$.

controlled solution as a whole possesses the lowest energy of any $q = 1$ solution.

To fully understand the meaning of hydraulic control, it is helpful to think about the way in which steady solutions can be established in the laboratory. The classical method, first used by Long (1954), is to tow an obstacle at speed u_0 through a long tank of fluid of equilibrium depth h_0. An observer moving with the obstacle then sees a steady flow established in the vicinity of the obstacle, and this steady state depends upon the ratio of obstacle height to initial depth b_m/h_0 and the Froud number $F_0 = u_0/(gh_0)^{1/2}$. Figure 5 (taken from Baines and Davies, 1980) shows the different steady flows that can occur, along with a sketch of the upstream-propagating disturbance which establishes the steady flow. When the towing speed is small enough so that $F_0 < 1$, there is a critical dimensionless obstacle height b_m/h_0 given by curve AB required to establish a controlled steady flow. To the left of this curve the flow adjusts to a subcritical solution and no choking or partial blocking occurs; that is, the depth upstream of the obstacle remains identical to the initial depth. To the right of AB, the upstream flow u_0 and h_0 (seen by the moving observer) has insufficient energy and flow force to surmount the sill. The result is that a bore forms which propagates upstream, producing a new upstream state with the minimum energy and flow force necessary to surmount the sill. Thus, the new flow is hydraulically controlled. If the obstacle height is large enough, the flow can be completely blocked; the critical b_m/h_0 required is given by line BC in Fig. 5. The curve AD in Fig. 5 divides flows having hydraulic jumps in the lee of an obstacle from flows without lee jumps.

When $F_0 > 1$, the situation is complicated by the fact that bores can become stationary (relative to the obstacle) in the upstream flow. The values of F_0 and b_m/h_0 for which this occurs are given by curve AF. Curve AE indicates values of F_0 and b_m/h_0 for which the approaching flow has the minimum energy necessary to surmount the sill and is the continuation of curve AB. In the area FAE it is possible to have either a controlled or noncontrolled flow, depending on how the obstacle is started from rest. The associated hysteresis is discussed by Pratt (1983) including a numerical example. Further discussion of the curves in Fig. 5 and their derivation will be given in section 4.

If one could imagine the deep circulation in a hypothetical flat-bottom ocean with no straits and sills, then the towing experiment results say something about the amount of topographic relief it would be necessary to introduce to hydraulically influence the circulation. Although the forcing mechanism is somewhat unrealistic, the transients excited as the flow adjusts to the obstacle are in many respects independent of the forcing. In fact, it can be shown (Houghton and Kasahara, 1968) that the adjustment excites the most general response possible within the context of shallow water

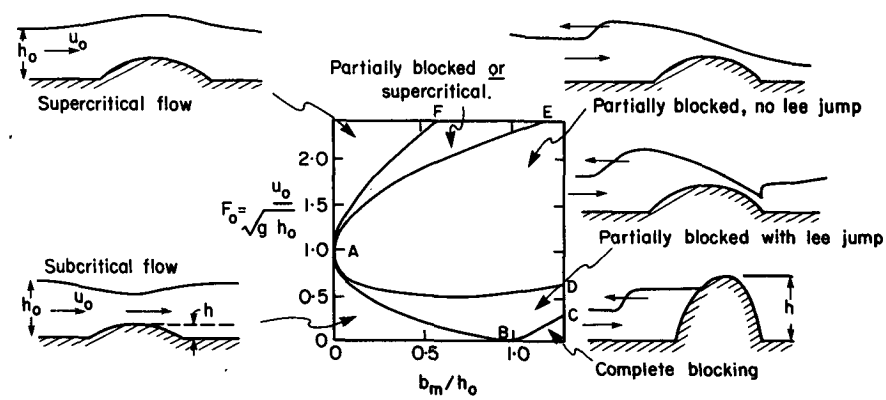

FIG. 5. Regime diagram showing the different steady flows established in the towing experiment. F_0 is the Froude number based on the towing speed u_0 and the equilibrium depth h_0, while b_m is the sill height (from Baines and Davies, 1980).

theory. Therefore, the results of the towing experiment provide valuable insight into the response to other types of forcing (see Pratt, 1984b).

3. Steady solutions with friction

Now reconsider the momentum equations (2.1) and (2.2) with nonzero C_d (and constant w). If u_x is eliminated between the two, a single equation for the variation in layer thickness is obtained:

$$\frac{dh}{dx} = \frac{db/dx + C_d F^2}{F^2 - 1} \tag{3.1}$$

where

$$F^2 = u^2/g^* h.$$

If the bottom is level ($db/dx = 0$), friction causes the layer thickness to increase ($dh/dx > 0$) in the direction of flow under supercritical ($F > 1$) conditions. When the flow is subcritical ($F < 1$), however, the thickness decreases (and the velocity increases) in the flow direction; that is, friction causes the flow to accelerate! This nonintuitive result can be made clearer if one considers the specific energy curve in Fig. 4. For a nonsloping bottom, the specific energy is essentially the energy or Bernoulli function and is conserved in the absence of friction. Suppose that an observer starts at point P on the subcritical branch of the energy curve in Fig. 4, corresponding to a dimensionless depth of 2.5. Since friction deletes energy from the flow, the observer must move to the left (toward P') on the energy curve as proceeding downstream, and this results in a decrease in layer thickness. The physical meaning of this result is as follows: when the flow is subcritical, the energy is composed primarily of potential energy, the proportion of kinetic energy being small. Thus energy can effectively be deleted from the flow only by deleting potential energy, i.e., decreasing the layer thickness.

Now consider the conditions which must hold in order that the flow be critical, $F = 1$. For frictionless flow it has already been shown that critical flow occurs only over the sill of the obstacle. In fact, this result can be obtained by setting $C_d = 0$ and $F = 1$ in (3.1). Clearly db/dx must be zero in order that dh/dx remain bounded. With nonzero C_d, (3.1) indicates that critical flow occurs at the position $x = x_c$ such that

$$db/dx|_{x=x_c} = -C_d. \tag{3.2}$$

This slope is known as the "critical slope."[2] Since C_d is positive, the point x_c of critical flow must lie on the downstream face of the obstacle where the bottom slope is negative. It should also be noted that the quadratic drag law does not alter the dynamical significance of the critical flow condition; the definition of the long-wave speed is unaltered by friction, and such waves continue to remain stationary when $u = (g^* h)^{1/2}$. Furthermore, since the arguments leading to (2.9) and (2.10) were based only on conservation of mass, critical flow occurs when the specific energy and flow force are at a minimum. Therefore, the features that associate critical flow with the process of hydraulic control are present regardless of quadratic friction.

It is interesting to speculate where critical flow might occur in the Iceland–Faroe overflow of Fig. 1. The downstream face of the ridge can be broken into three sections having slopes of about 0.002, 0.003, and 0.01 respectively, as shown. If the overflow was frictionless, critical flow would occur at the sill located near the 275 km mark on the horizontal scale. A drag coefficient of 0.002 would indicate that critical flow could occur 0–15 km downstream of the sill, while $C_d = 0.003$ would indicate a point 15–60 km downstream of the sill. Of course, this computation neglects the effects of width variations, the earth's rotation, and other factors that may influence the hydraulics of this overflow but are difficult to estimate.

Now consider the steady solutions obtained by fixing the dimensionless flow rate at value $q = 1$ and varying the energy B_1 of the flow immediately upstream of the obstacle, as before. The resulting interfacial profiles are shown in Fig. 6. The topography here is given by (2.6) and the friction parameter α has value 0.5. The subcritical solution (curve A–A', $B_1 = 3.25$) experiences a net decrease in elevation across the obstacle, as suggested by the remarks at the beginning of this section. In fact, an indiscriminate observer might be misled by the solution's asymmetry into thinking that this solution is hydraulically controlled. Decreasing B_1 to the value 3.10 leads to the hydraulically controlled profile B–B'. A larger value of B_1 than in the inviscid case (Fig. 3) is required for this controlled flow since the fluid

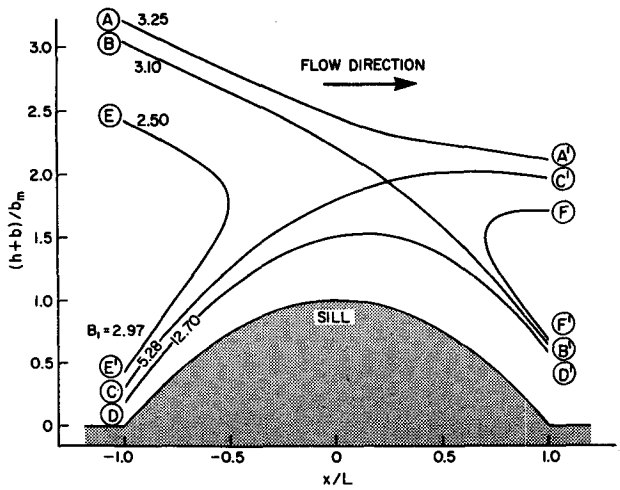

FIG. 6. As in Fig. 3 but with $\alpha = 0.5$. Note that the Bernoulli function B_1 is not conserved as in Fig. 3. Here B_1 represents the energy measured at $x/L = -1$.

[2] When channel width variations occur, (3.2) is generalized to $(db/dx)|_{x=x_c} - (hw^{-1}dw/dx)|_{x=x_c} = -C_d$.

must overcome both an elevation change and a drag to surmount the obstacle. The location x_c/L of the critical or control point can be predicted by using (3.2) in (2.6), with the result

$$x_c/L = \alpha/2, \quad |x| < L. \tag{3.3}$$

For $\alpha = 0.5$ we have $x_c/L = 0.25$ and this marks the location where intersection with the curve C–C′ occurs in Fig. 6. At the sill the Froude number of the hydraulically controlled flow is 0.76, and one could easily be misled by this value into thinking that the flow is of type A–A′. To be certain, one must measure the Froude number at the location given by (3.3).

Some other examples of hydraulically driven, frictional flow can be found in the literature; among them are flow down an incline of constant slope (Turner, 1973) and tidally forced subcritical flow through a weirlike constriction (Stiegebrandt, 1980). In particular, Turner discusses qualitatively how the flow can change from subcritical to supercritical, and vice versa, over a uniform slope, and his Eq. (3.2.8) is essentially my Eq. (3.1).

4. The initial value problem

I now discuss the effect of friction on the establishment of steady solutions. Figure 7 shows the transients that established hydraulically controlled states in the previously discussed towing experiment. The figure is drawn in a reference frame moving with the speed u_0 of the obstacle. To the left of the obstacle a bore moves upstream, partially blocking the flow. A stationary hydraulic jump is shown on the downstream face of the obstacle, and a rarefaction wave propagates downstream to the right of the jump. For sufficiently large towing speed, the hydraulic jump can move off the obstacle and propagate downstream as a bore. Far upstream and downstream the depth is just the undisturbed depth h_0. If this depth is known, along with the obstacle height b_m and towing speed u_0, it is possible to compute the entire transient flow field using shock-joining theory.

How does friction affect the flow field shown in Fig. 7? First of all, friction will have no effect on the far-field u_0 and h_0, since this part of the flow is at rest relative to the flat bottom. Friction should also have no effect on the type of transients excited, since these transients constitute the most general response allowable in shallow water theory, regardless of the value of α. On the other hand, friction will certainly alter the segments of steady flow that occur in the near field (roughly between sections 1 and 3 in Fig. 7). One would expect friction to be strongest in the shallow region over the obstacle with weaker frictional effects in the subcritical flow upstream of the obstacle and downstream of the jump.

In fact, if the fluid depth away from the obstacle is sufficiently large, it should be possible to neglect friction there. Following an argument similar to the one used by Stigebrandt (1980), suppose that h_1 and u_1 are scales for the layer thickness and velocity away from the obstacle. If this flow is subcritical, the primary momentum balance will be between the terms g^*dh/dx and $C_d u^2/h$ in (2.1), and this balance suggests that the friction will change the layer thickness over the horizontal length

$$\lambda = g^* h_1^2 / C_d u_1^2.$$

If this length is small compared to the characteristic obstacle length L, then one should be able to ignore friction away from the obstacle to a first approximation. Using $u_1^2 = Q^2/w^2 h_1^2 = g^* h_c^3 / h_1^2$, where h_c denotes the critical layer thickness, the approximation is equivalent to

$$\frac{L}{\lambda} = \left(\frac{LC_d}{h_1}\right)\left(\frac{h_c}{h_1}\right)^3 \ll 1. \tag{4.1}$$

For the Iceland–Faroe overflow (Fig. 1) let $L = 4 \times 10^5$ m, $h_1 = 500$ m, $h_c = 50$ m and $C_d = 0.003$, giving $L/\lambda = 2.4 \times 10^{-3}$.

Under the condition (4.1) the adjustment of a resting fluid to a towed obstacle will proceed as follows. There will be an initial adjustment, the time scale of which will be roughly $L/(g^* h_0)^{1/2}$, the time required for a gravity wave to traverse the obstacle. During this initial phase, blocking bores and rarefactions form and move away from the obstacle, leaving behind a nearly steady flow, as in Fig. 7. Although some interfacial slope will develop away from the obstacle, this slope will be negligible compared to the hydraulically and frictionally induced slopes over the obstacle. It is this initial adjustment that will be computed here. After a time

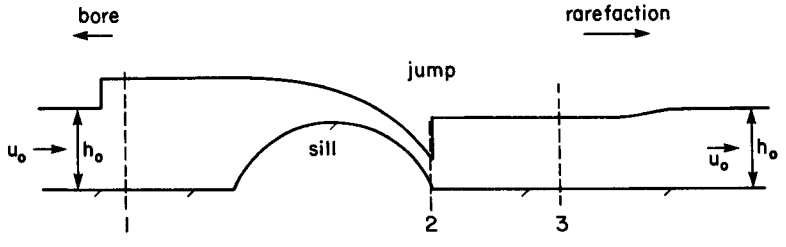

FIG. 7. Sketch of the blocking bore, hydraulic jump, and rarefaction wave that develop when critically controlled flow is established in the towing experiment.

$\lambda/(g^*h_0)^{1/2}$ the cumulative effect of friction away from the obstacle may become as important as the obstacle itself in determining a solution. However, in most laboratory and oceanographic situations of importance, other complications (such as reflections from basin walls) will intervene before friction does.

In order to maintain the greatest degree of simplicity, I will work with an obstacle of parabolic shape as given by (2.6). This shape contains the single horizontal length scale L, and friction will enter the problem through the single parameter $\alpha = C_dL/b_m$. First consider Eqs. (2.3) and (2.4) for the steady flow over the obstacle, rewritten here as

$$u^2(x)/2 + g^*[h(x) + b(x)]$$

$$= u_1^2/2 + g^*h_1 - C_d\int_{-L}^{x}[u^2(\hat{x})/h(\hat{x})]d\hat{x} \quad (4.2)$$

$$u(x)h(x) = u_1h_1. \quad (4.3)$$

The subscript 1 denotes a value measured upstream of the obstacle but downstream of the blocking bore, as shown in Fig. 7. The flow u_0 and h_0 far upstream is connected to u_1 and h_1 through the Rankine–Hugoniot conditions of mass and momentum conservation:

$$c(h_0 - h_1) = u_0h_0 - u_1h_1 \quad (4.4)$$

$$c = u_0 - [g^*h_1(h_1 + h_0)/2h_0]^{1/2} \quad (4.5)$$

where c is the bore speed. Downstream of the obstacle, u_2 and h_2 can be connected to u_3 and h_3 across the jump using relationships of the same form as (4.4) and (4.5). Finally, u_3 and h_3 can be connected to u_0 and h_0 across the rarefaction wave using conservation of the Riemann invariant:

$$u_3 - 2(g^*h_3)^{1/2} = u_0 - 2(g^*h_0)^{1/2}. \quad (4.6)$$

[See Stoker (1957) for a thorough discussion of this condition and (4.4)–(4.5).]

In addition, (3.3) indicates that critical flow will occur at location $x_c/L = \alpha/2$, corresponding to obstacle elevation

$$b_c = b_m(1 - \alpha^2/4). \quad (4.7)$$

Note that critical flow can occur only for values of $\alpha \leq 2$; for larger values the bottom slope will be too small to satisfy (3.2).

Where jumps and bores occur, mass and momentum flux may be exchanged between layers, and, strictly speaking, (4.4) and (4.5) should be modified to include these effects. However, the correct forms of these modifications are not well established, particularly with regard to the question of entrainment of mass. Furthermore, the experiments upon which Fig. 5 are based were done with a single-layer system in which (4.4) and (4.5) hold. To make comparisons with these results and to maintain the goal of illustrating only gross changes due to friction, I will neglect upper-layer interactions and use (4.4) and (4.5) as they are.

a. The curve BAE

The curve BAE of Fig. 5 (due to Long, 1954) indicates the threshold obstacle height above which u_0 and h_0 are insufficient to allow inviscid fluid to surmount the obstacle in a steady state. It is also the curve for which the amplitude $h_1 - h_0$ of the blocking bore in Fig. 7 is zero. That is, the curve is determined by those values of u_0 and h_0 that specify the upstream state of a steady flow which becomes critical over the obstacle. Evaluating (4.2) and (4.3) at $x = x_c$ and setting $u_0 = u_1$ and $h_0 = h_1$ gives

$$\tfrac{3}{2}g^*h_c + g^*b_m(1 - \alpha^2/4)$$

$$= u_0^2/2 + g^*h_0 - C_d\int_{-L}^{x_c}[u^2(\hat{x})/h(\hat{x})]d\hat{x} \quad (4.8)$$

$$u_0h_0 = g^{*1/2}h_c^{3/2}. \quad (4.9)$$

Eliminating u_0 between these equations and dividing the result by g^*h_0 leads, after some rearrangement of terms, to

$$b_m/h_0 = 1 - \tfrac{3}{2}F_0^{2/3} + \tfrac{1}{2}F_0^2 + \tfrac{1}{2}\alpha(b_m/h_0)$$

$$\times\left\{\frac{\alpha}{2} - F_0^2\int_{-1}^{\alpha/2}[h_0/h(x/L)]^3d(x/L)\right\}. \quad (4.10)$$

Setting $\alpha = 0$ in (4.10) gives the inviscid curve BAE. For finite α, (4.10) shows that the threshold obstacle height b_m/h_0 is altered by two competing effects. The first, associated with the term $\alpha^2(b_m/h_0)/4$, is due to the movement of the critical point (or control point) to a lower elevation, and this movement tends to increase the threshold height. The second effect, associated with the integral in (4.10), is the frictional drag caused by that portion of the obstacle upstream of x_c. This drag tends to decrease the threshold height.

Figure 8 shows how the curve BAE is altered when α has its maximum possible value (=2.0). The new (dashed) curve has been obtained by solving (4.10) numerically and the algorithm is described in appendix B. Apparently, the drag effect mentioned above is always larger than the critical point displacement effect, since the b_m/h_0 required to cause partial blocking is decreased by friction. This decrease is not dramatic when $F_0 < 1$ but is huge when $F_0 > 1$, due to the greater influence of friction under supercritical conditions. Note that no shock joining has been employed to obtain these curves, so the results are valid for both the single-layer and the two-layer (reduced gravity) models.

To the right of the dashed curve BAE′ in Fig. 8, the flow u_0 and h_0 (seen in the moving frame) has insufficient energy and flow force to surmount the obstacle. Partial blocking of this flow will result, leading to a critically controlled state. To the left of this curve there

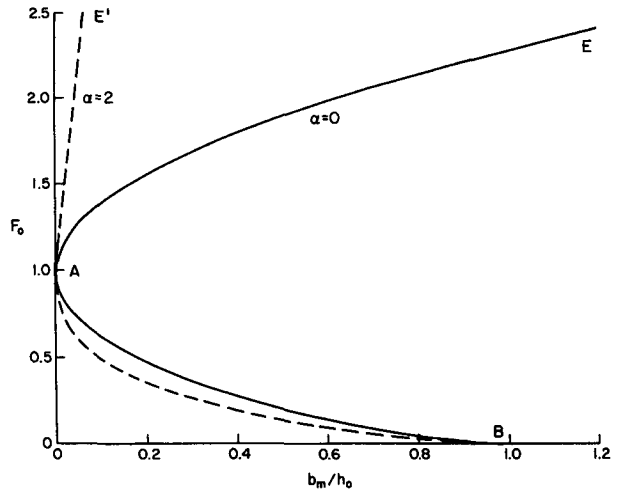

FIG. 8. The threshold obstacle height curve for $\alpha = 0$ and $\alpha = 2$. To the right of this curve, a steady flow of upstream Froude number F_0 has insufficient energy and flow force to surmount the obstacle.

may be a slight blocking effect due to frictional drag, but the flow nevertheless has sufficient energy to surmount the obstacle, and a noncontrolled steady state will be established.

b. The curve AF

The curve AF of Fig. 5 (due to Long, 1970) marks those values of F_0 and b_m/h_0 for which the upstream blocking bore is stationary. For finite α the curve can be calculated as follows. Proceeding as in section 4a, evaluate (4.2) and (4.3) at $x = x_c$ and combine the results, obtaining

$$b_m/h_1 = 1 - \frac{3}{2}F_1^{2/3} + \frac{1}{2}F_1^2 + \frac{1}{2}\alpha(b_m/h_1) \times \left\{\frac{\alpha}{2} - F_0^2 \int_{-1}^{\alpha/2} [h_1/h(x/L)]^3 d(x/L)\right\}. \quad (4.11)$$

Also, setting the bore speed $c = 0$ in (4.4) and (4.5) and combining the results gives the relationship,

$$(h_1/h_0) = [1 + (1 + 8F_1^2)^{1/2}]/(4F_1^2). \quad (4.12)$$

To find a point $(b_m/h_0, F_0)$ for which the blocking bore is stationary, first choose a value for F_1 and use (4.11) and (4.12) to find b_m/h_1 and h_1/h_0. Finally, compute b_m/h_0 and F_0 from

$$b_m/h_0 = (b_m/h_1)(h_1/h_0) \quad (4.13a)$$

$$F_0 = F_1(h_1/h_0)^{3/2} \quad (4.13b)$$

(the latter follows from 4.4). See appendix B for more details.

Figure 9 shows the curve AF, along with its $\alpha = 2.0$ counterpart, labeled AF'. Also shown are the curves AE and AE', indicating the threshold obstacle height for $\alpha = 0$ and $\alpha = 2$ based on energy (or flow force) considerations. First consider the significance of the inviscid curves AF and AE. In the shaded region FAE, the outcome of the towing experiment depends upon *how* the towing is initiated. Suppose one initiates the towing experiment by arranging for b_m/h_0 and F_0 to lie at point p in Fig. 9. Then no partial blockage occurs and a steady supercritical flow will develop over the obstacle. If F_0 is then decreased by decreasing the towing speed so that the point p' is reached, the flow will continue to be supercritical over the obstacle. Further lowering F_0 until point p'' is reached *does* result in the formation of a blocking bore, and this bore moves upstream, leaving behind a critically controlled flow over the obstacle. However, if F_0 is now increased back to the value indicated at point p', the bore continues to move upstream and the critically controlled state is maintained. To reestablish a supercritical flow it is necessary to raise F_0 above the line AF, wait for the bore to return to the obstacle, and then lower F_0 back to its value at p'. (For a numerical example of a similar chain of events, the reader is referred to Pratt, 1983.)

Now consider the shaded region E'AF' for $\alpha = 2.0$ and note that the stationary bore curve AF' lies *to the right* of the threshold curve AE'. Thus, if one begins at point q and moves to q', partial blockage is initiated because the flow at q' has insufficient energy to surmount the obstacle. However, the blocking bore will be unable to move upstream, as q' lies to the left of the stationary bore curve AF'. Apparently, the only possible outcome is that the bore remains stationary *over* the upstream face of the obstacle (a feature not possible under frictionless conditions). There will be a unique

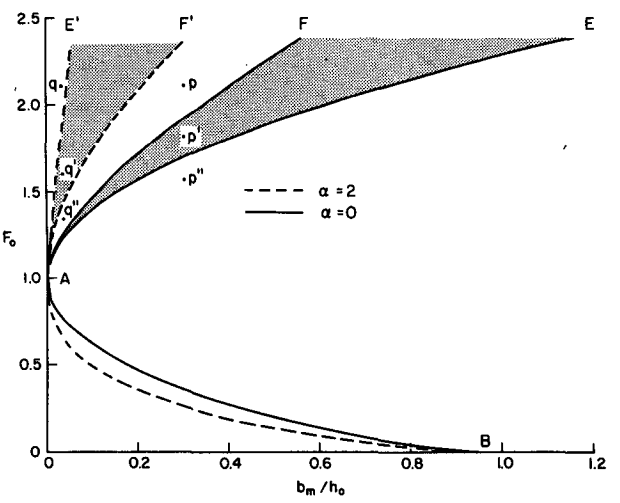

FIG. 9. Curves AF ($\alpha = 0$) and AF' ($\alpha = 2$) indicate steady flow with stationary upstream bores. The curves EAB and E'AB are as in Fig. 8. Hysteresis occurs in the shaded area EAF. In region E'AF' stationary bores occur on the upstream face of the obstacle and there is no hysteresis.

position for this stationary bore determined by F_0 and b_m/h_0. If one moves from q' to q'', the bore moves upstream. Returning to q' will cause the bore to become stationary again at the predetermined position. Thus, multiple steady states are apparently not possible in region E'AF'.

c. *The curve AD*

The curve AD of Fig. 5 (due to Houghton and Kasahara, 1968) gives those values of F_0 and b_m/h_0 for which the hydraulic jump remains stationary at the downstream edge $x = L$ of the obstacle, as shown in Fig. 7. Below the curve AD, jumps lie on the sloping portion of the obstacle, $0 < x < L$; whereas above the curve, jumps propagate downstream. Calculating the curve requires quite a bit of algebra, and I leave the details to appendix C. Briefly, one starts by assuming that a steady flow exists over the obstacle and that a stationary jump exists at $x = L$. Using Fig. 7 as a model, one then constructs the different segments of the flow field using the steady flow equations (4.2) and (4.3) and the shock-joining conditions (4.4)–(4.6).

The change in curve AD that occurs when $\alpha = 1$ and $\alpha = 2$ is shown by the solid curves in Fig. 10. Note that increasing α tends to raise this curve, thereby enlarging the parameter space in which lee jumps occur. Conversely, increasing α moves the control point downstream, thereby decreasing the distance over which stationary jumps occur. The result is a decrease in the amplitude $h_3 - h_2$ that the stationary jump can have. The limiting case is $\alpha = 2$; here the flow is critical at $x = L$ and any jump must have zero amplitude [see Eq. (4.12)]. The dashed curves in Fig. 10 give the dimensionless amplitude $(h_3 - h_2)/h_1$ of the stationary jump when the jump lies at $x = L$. If one picks values

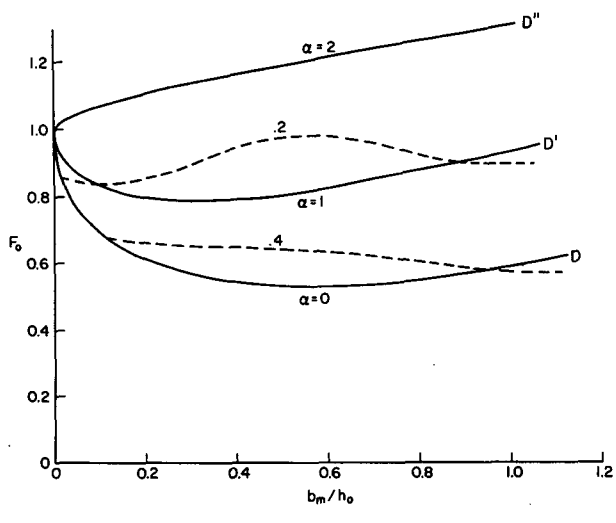

FIG. 10. The solid lines indicate values of F_0 and b_m/h_0 for which a stationary jump exists at $x = L$. Results are plotted for $\alpha = 0$, 1 and 2. The dashed curves are contours of the dimensionless amplitude $(h_3 - h_2)/h_1$ of the jump at $x = L$.

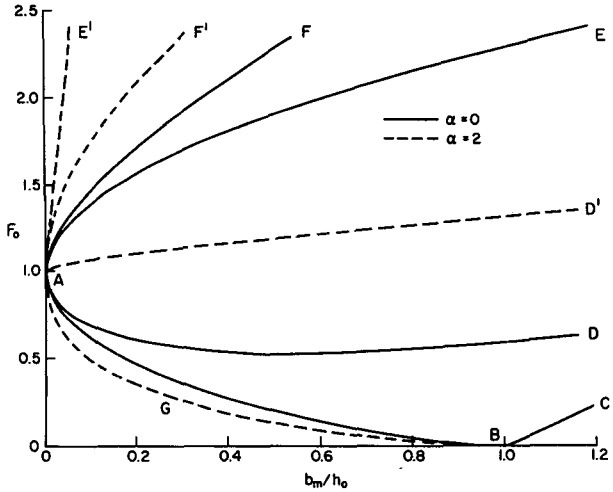

FIG. 11. The towing experiment regime diagram for $\alpha = 0$ and $\alpha = 2$ (cf. Fig. 5).

of b_m/h_0 and F_0, then the corresponding α read from the solid curves in Fig. 10 gives the friction parameter necessary to establish a stationary jump at $x = L$. The dashed curves give the amplitude of this jump, representing the maximum amplitude that any stationary jump can have at the given b_m/h_0 and F_0. For fixed b_m/h_0 (or F_0) this maximum amplitude decreases with increasing α.

d. *The curve AC*

This curve gives the obstacle height needed to completely block the flow. Since the steady state that forms near the obstacle is one of no motion, friction plays no role and the curve AC is independent of α.

5. Discussion

Although many of the well-established, basic ideas concerning hydraulic control, critical flow, and energy and flow force minimization remain essentially unaltered by the inclusion of the quadratic drag law, many quantitative alterations take place. One is the displacement downstream of the control point, as determined by (3.2). It has been suggested that such a control point could lie as far as 60 km downstream of the sill in the Iceland–Faroe Channel. If the drag coefficient is so large that (3.2) cannot be satisfied, the flow cannot be critically controlled and friction completely dominates hydraulic effects. Friction also gives rise to asymmetries in the interface profiles that can cause, among other things, subcritical solutions to resemble controlled solutions.

It is also possible to predict how friction influences the outcome of the classical towing experiment under the approximation (4.1). Figure 11 summarizes these findings by showing the flow regimes that occur for

given (b_m/h_0, F_0) in the frictionless case $\alpha = 0$ and the case of strongest allowable friction $\alpha = 2$. Although friction does not affect the minimum obstacle height required to completely block the flow (curve BC), it decreases the minimum obstacle height required to produce hydraulically induced partial blocking (curve EAB versus E'AGB). Friction also enlarges the parameter space in which lee hydraulic jumps occur (area DABC versus D'ABC) and apparently can give rise to a new region (area E'AF') in which stationary bores occur on the upstream face of the obstacle.

One question unanswered by the present study concerns the case $\alpha > 2$. What is the nature of the adjustment that occurs in this friction-dominated case and can the approximation allowing neglect of friction away from the obstacle still be made?

Acknowledgments. This work was supported by the National Science Foundation under Grant OCE85-15655. The author wishes to thank Peter Baines and the reviewers for their constructive comments and Mary Ann Lucas for typing the manuscript.

APPENDIX A

Numerical Method for Solving (2.5)

Using the trapezoidal rule, the integral in (2.5) can be approximated as

$$\int_{-1}^{(x+\Delta x)/L} (b_m/h)^3 d(x/L) = \int_{-1}^{x/L} (b_m/h)^3 d(x/L) + \frac{\Delta x}{2L}\left[\left(\frac{b_m}{h(x)}\right)^3 + \left(\frac{b_m}{h(x+\Delta x)}\right)^3\right]. \quad \text{(A1)}$$

Substituting (A1) and (2.6) into (2.5) and evaluating the result at $x + \Delta x$ leads to the quartic equation

$$\tilde{h}_{n+1}^4 + \left[1 - \xi_{n+1}^2 + \tfrac{1}{2}\alpha q^2(\xi_{n+1} - \xi_n)\tilde{h}_n^{-3} - B_n\right]\tilde{h}_{n+1}^3 + \tfrac{1}{2}q^2\tilde{h}_{n+1} + \tfrac{1}{2}\alpha q^2(\xi_{n+1} - \xi_n) = 0 \quad \text{(A2)}$$

where

$$\xi_n = x_n/L, \quad x_{n+1} = x_n + \Delta x, \quad \tilde{h}_n = h(x_n)/b_m$$

$$B_n = \tilde{h}(-1) + \tfrac{1}{2}q^2/\tilde{h}^2(-1) - \tfrac{1}{2}\alpha q^2 \sum_{i=1}^{n} (\xi_i - \xi_{i-1})(\tilde{h}_i^{-3} + \tilde{h}_{i-1}^{-3}). \quad \text{(A3)}$$

To compute $\tilde{h}(\xi)$ over the parabolic obstacle for given q and B_0, start at the upstream edge $\xi = -1$. To find $\tilde{h}(\xi = -1)$, substitute $n = 0$, $\xi_{n+1} = \xi_n = -1$ and $B_n = B_0$ into (A2) and solve for $\tilde{h}_1$. (At most, two real positive roots will occur, corresponding to subcritical and supercritical solutions. If only one real positive root occurs the flow is critical. If none occur, B_0 must be increased.) Next, set $n = 1$, $B_n = B_0$; solve for $\tilde{h}_2 = \tilde{h}(-1 + \Delta\xi)$; calculate B_1 from (A3); set $n = 2$ and reiterate. All profiles in Fig. 3 except B–B' and C–C' were calculated using $\Delta\xi = \xi_{n+1} - \xi_n = 0.02$. More resolution is needed to calculate B–B' and C–C', and $\Delta\xi = 0.005$ was used.

APPENDIX B

Numerical Method for Calculating the Curves of Figs. 8 and 9

Curve E'AB is calculated by solving (4.10) for b_m/h_0 with given α and F_0. The procedure is to first guess b_m/h_0. [A good first guess may be obtained by setting $\alpha = 0$ and solving (4.10) directly.] Using this guess, evaluate the integral in (4.10). To do so, it is necessary to calculate the depth profile from $x = -L$ to $x = x_c$ over the parabolic obstacle by integrating (2.1) from position x to x_c. The result can be obtained simply by replacing u_0, h_0, and $-L$ by $u(x)$, $h(x)$, and x in (4.8) and (4.9). The results of these substitutions can then be combined, yielding

$$\tfrac{1}{2}F_0^2\hat{h}^{-2} + \hat{h} + (b_m/h_0)(1 - \xi^2) = \tfrac{3}{2}F_0^{2/3} + (b_m/h_0)(1 - \alpha^2/4) + \alpha F_0^2(b_m/h_0)\int_{\xi}^{\alpha/2} \hat{h}^{-3} d\xi' \quad \text{(B1)}$$

where $\hat{h} = h/h_0$, $\xi = x/L$, and the relation $\hat{h}_c = F_0^{2/3}$ is used. Proceeding as in appendix A, one applies the trapezoidal rule to the integral, yielding the quartic equation

$$\hat{h}_{n+1}^4 + [(b_m/h_0)(\alpha^2/4 - \xi^2) - \tfrac{1}{2}\alpha F_0^2(b_m/h_0)(\xi_n - \xi_{n-1})\hat{h}_n^{-3} - \hat{B}_n]\hat{h}_{n+1}^{-3} + \tfrac{1}{2}F_0^2\hat{h} - \tfrac{1}{2}\alpha F_0^2(b_m/h_0)(\xi_n - \xi_{n-1}) = 0 \quad \text{(B2)}$$

where

$$\hat{B}_n = \tfrac{3}{2}F_0^{2/3} + \tfrac{1}{2}\alpha F_0^2(b_m/h_0)\sum_{i=2}^{n}(\xi_i - \xi_{i-1})(\hat{h}_i^{-3} + \hat{h}_{i-1}^{-3}) \quad \text{(B3)}$$

and where ξ_n is as defined in appendix A. Starting with $n = 1$, $\xi_n = x_c/L = \alpha/2$, $\xi_{n+1} = \xi_n - \Delta\xi$, $\hat{B}_n = \frac{3}{2}F_0^{2/3}$, and $\hat{h}_n = F_0^{2/3}$, calculate $\hat{h}_{n+1}$ from (B2). Then set $n = 2$, calculate $\hat{B}_n$ from (B3) and reiterate, working backward toward the upstream edge $\xi = -1$ of the obstacle. When $\xi = 1$ is reached, the value $\hat{B}_n - \frac{3}{2}F_0^{2/3}$ approximates the value of the integral in (4.10). If this value, the guessed value of b_m/h_0, and the given values of F_0 and α are substituted into the right-hand side of (4.10), the result gives a new estimate of b_m/h_0.

Using $\Delta\xi = 0.02$, the above procedure was used to construct curve E'AB in Fig. 8. For $F_0 < 0.5$, it is only necessary to iterate b_m/h_0 three or four times to obtain

a solution accurate to 1%. For $F_0 > 0.5$, as many as ten iterations were sometimes necessary.

To calculate the curves of Fig. 9, one first chooses values α and F_1 and computes b_m/h_1 using the above procedure. Next the shock-joining conditions (4.13) are used to calculate F_0 and h_0/h_1, giving a point on the appropriate F_0 versus b_0/h_0 curve of Fig. 9.

APPENDIX C

Numerical Method for Calculating Curves in Fig. 10

To calculate curves A–D, A–D′, and A–D″ in Fig. 10, specify F_1 and calculate a corresponding value of b_m/h_1 using the method of appendix B. Next, use Eq. (B3) with F_0 and h_0 replaced by F_1 and h_1 to find the fluid depth h_2/h_1 at the foot of the obstacle. The corresponding Froude number F_2 is given by conservation of mass as $F_1(h_1/h_2)^{3/2}$. Following Fig. 7, the depth and Froude number h_3/h_1 and F_3 on the downstream side of the hydraulic jump can be computed from the shock-joining conditions

$$h_2/h_3 = (F_3/F_2)^{2/3} \tag{C1}$$

$$F_3^{2/3} = [1 + (1 + 8F_2^2)^{1/2}]/4F_2^{4/3}. \tag{C2}$$

Finally, it is possible to eliminate c and u_0 from Eqs. (4.4)–(4.6), resulting in the following equation for $\tilde{h}_0 = h_0/h_1$

$$\tilde{h}_0^3 - 9\tilde{h}_0^2 - 8A\tilde{h}_0^{3/2} - (2A^2 + 1)\tilde{h}_0 + 1 = 0 \tag{C3}$$

where

$$A = F_1(\tilde{h}_3^{-1/2} - 1) - 2\tilde{h}_3^{1/2}, \quad \tilde{h}_3 = h_3/h_1.$$

Using the value of $\tilde{h}_3$ computed from (C1) and (C2), only one physically realizable root of (C3) can be found. Once $\tilde{h}_0$ is known, one can compute $b_m/h_0 = (b_m/h_1)/\tilde{h}_0$. Also, Eq. (4.6) can be rearranged, yielding

$$F_0 = 2[1 - (\tilde{h}_3/\tilde{h}_0)^{1/2}] + F_3(\tilde{h}_3/\tilde{h}_0)^{1/2}.$$

The result is that one point $(F_0, b_m/h_0)$ on the desired curve is obtained.

REFERENCES

Armi, L., and D. Farmer, 1984: The internal hydraulics of the Strait of Gibraltar and associated sills and narrows. *Oceanol. Acta,* **8,** 37–46.

Baines, P. G., 1984. A unified description of two-layer flow over topography. *J. Fluid Mech.,* **146,** 127–167.

——, and P. A. Davies, 1980: Laboratory studies of topography effects in rotating and/or stratified fluids. *Orographic Effects in Planetary Flows.* GARP Publ. Ser. No. 23, 762 pp.

Farmer, D. M., and R. A. Denton, 1985: Hydraulic control of flow over the sill in Observatory Inlet. *J. Geophys. Res.–Oceans,* **90,** 9051–9068.

Grant, A. B., 1968: *Atlas of Oceanographic Sections, Davis Strait–Labrator Basin–Denmark Strait 1965–1967.* Atlantic Oceanographic Laboratory, Bedford Institute, unpublished manuscript, 140 pp.

Grant, W. D., A. J. Williams and S. M. Glenn, 1984. Bottom stress estimates and their prediction on the northern California continental shelf during CODE-1: The importance of wave–current interaction. *J. Phys. Oceanogr.,* **14,** 489–648.

Hansen, B., and J. Meincke, 1979. Eddies and meanders in the Iceland–Faroe Ridge area. *Deep-Sea Res.,* **26A,** 1067–1082.

Hogg, Nelson G., 1983. Hydraulic control and flow separation in a multilayered fluid with applications to the Vema Channel. *J. Phys. Oceanogr.,* **13,** 695–708.

Houghton, D. D., and A. Kasahara, 1968. Nonlinear shallow fluid flow over an isolated ridge. *Commun. Pure Appl. Math.,* **21,** 1–23.

Lacombe, H., and C. Richez, 1982. The regime of the Strait of Gibraltar. *Hydrodynamics of Semi-enclosed Seas,* J. C. J. Nihol, Ed., Elsevier Oceanogr. Ser., **34,** 13–73.

Lawrence, G. A., 1985: The hydraulics and mixing of two-layer flow over an obstacle. University of California, Berkeley, Ph.D. dissertation, 122 pp.

Long, R. R., 1954: Some aspects of the flow of stratified fluids. II. Experiments with a two-fluid system. *Tellus,* **6,** 97–115.

——, 1970. Blocking effects in flow over obstacles. *Tellus,* **22,** 471–480.

Lonsdale, P., 1977. Inflow of bottom water to the Panama Basin. *Deep-Sea Res.,* **24,** 1065–1101.

Pratt, L. J., 1983. A note on nonlinear flow over an obstacle. *Geophys. Astrophys. Fluid Dyn.,* **24,** 63–68.

——, 1984a. Nonlinear flow with multiple obstructions. *J. Atmos. Sci.,* **41,** 1214–1225.

——, 1984b. A time-dependent aspect of hydraulic control in Straits. *J. Phys. Oceanogr.,* **14,** 1414–1418.

Stigebrandt, A., 1980. Some aspects of tidal interaction with Fjord constrictions. *Estuarine Coastal Mar. Sci.,* **11,** 151–166.

——, 1984. The North Pacific: A global-scale estuary. *J. Phys. Oceanogr.,* **14,** 464–470.

Stoker, J. J., 1957. *Water Waves.* Interscience, 567 pp.

Stommel, H., and H. G. Farmer, 1952. Abrupt change in width in two-layer open channel flow. *J. Mar. Res.,* **11,** 205–214.

Tolmazin, D., 1977. Hydrological and hydrochemical structures in the areas of hypoxia and anoxia of the northwestern Black Sea. *Biol. Morya,* **43,** 12–17.

Turner, J. S., 1973. *Buoyancy Effects in Fluids.* Cambridge University Press, 367 pp.

Walin, G., and O. Petren, 1976. Some observations of the deep-flow in the Bornholm Strait during the period June 1973–December 1974. *Tellus,* **23,** 74–87.